JOURNAL OF APPLIED SCIENCES RESEARCH

JOURNAL home page: http://www.aensiweb.com/jasr.html 2013 December; 9(10): pages 6373-6386.

Published Online :15 January 2014 **Research Article**

Structural Pattern and Crustal Modeling of the Central Northern Part of Egypt, Using Bouguer Gravity Data

[1]Saada, S.A., [2]Zahra, H. and [3]El-Khadragy, A.A.

[1]Faculty of Science, Geology Department, Suez University, Suez, Egypt.
[2]Faculty of Science, Geology Department, Banha University, Banha, Egypt.
[3]Faculty of Science, Geology Department, Zagazig University. Zagazig, Egypt.

Received: 12 November 2013; **Revised:** 14 December, 2013; **Accepted:** 20 December 2013.

ABSTRACT

The aim of the present study is to investigate the crust and upper mantle of the central northern part of Egypt, using Bouguer gravity data. To achieve this aim, the gravity data have been subjected to modeling and interpretation. Analysis of the gravity data includes regional-residual separation technique utilizing the least-squares polynomial. Moreover, depth determination to the basement surface for the gravity anomalies is applied using the spectral analysis technique. The gravity data were integrated with the available geological well data and geophysical information to build up two-dimensional (2-D) crustal geologic models taken along the S - N direction across the study area. Consequently, three depth maps for the basement surface, Conrad and Moho discontinuities are constructed. These maps and models enable us to conclude that, 1) The densities of the rock units in the investigated area are; 2.1, 2.5, 2.7, 2.93 and 3.3 gr/cm^3 for the upper and lower sedimentary cover, upper crust (granitic layer) and lower crust (basaltic layer), and upper mantle, respectively. 2) The basement surface ranges between 1 km in the southwestern pat and 10 km in the northeastern part, the Conrad discontinuity occurs at a depth varies from 13.5 to 25 km from north to south, and the Mohorovicic discontinuity ranges approximately between 20 at the northern area and 35 km at the southern one. Euler deconvolution technique is applied to locate the step-faults and to determine their depths. Finally, a structural tectonic map was constructed using the available analytical data. It shows that, the area is affected by a large number of normal faults trending in an ENE trend intersected by a NNW trend forming uplifted and down-lifted blocks with step-faulted blocks in parts.

Key words: Crust, upper mantle, structural pattern, modeling and interpretation.

INTRODUCTION

The study area lies between Latitudes 28° 22' & 31°45' N and Longitudes 28° 30' & 33° 06' E (Fig. l). This area starts from the south of El Fayoum to the west and El Galala El Baharyia to the east, and extends northerly up to the Mediterranean offshore part and coveres a surface area of about 165000 km^2.

It comprises both of important prospective oil and gas provinces in Egypt. The main targets of this study include: (1) Outlining the geologic set-up and the structural features affecting the basement rocks and the overlying sedimentary cover, (2) Delineating the configurations of the basement surface, Conrad, as well as Moho discontinuities. (3)Throwing more lights on the tectonic regime. Accordingly, many techniques are applied on the available geological and geophysical data to achieve these aims.

The available geologic data consist of 46 wells reached to the basement surface, while the geophysical data include the Bouguer gravity anomaly map, with a scale of 1:500,000 and a contour interval of 2 mGal after EGPC, 1980, as shown in (Fig. 2).

The potential field data represented by gravity are subjected to both qualitative and quantitative techniques of interpretations. The analytical techniques applied on the Bouguer gravity anomaly map include trend analysis to define the major tectonic trends affecting the buried basement rocks, as well as the sedimentary cover using Afleck's [6] technique. Regional -residual separation is applied using the least-squares polynomial method [3], from the first to the seventh orders. In addition, a correlation coefficient is used to determine the optimum order [5]. Depth estimation to the basement surface is carried out on 19 gravity profiles, using the spectral analysis technique [44]. Euler deconvolution technique is used to locate the step-faults and to determine their depths. Moreover, two- dimensional modeling (2D) along three profiles is carried out to show the subsurface basement, Conrad and Moho discontinuities configurations. By digitizing these profiles, as well as two profiles after Salem *et al*. [41], the Conrad and Moho discontinuities maps are constructed. Further, a basement structure map is constructed, using all the interpreted results.

Corresponding Author: Saada, S.A., Faculty of Science, Geology Department, Suez University, Suez, Egypt.

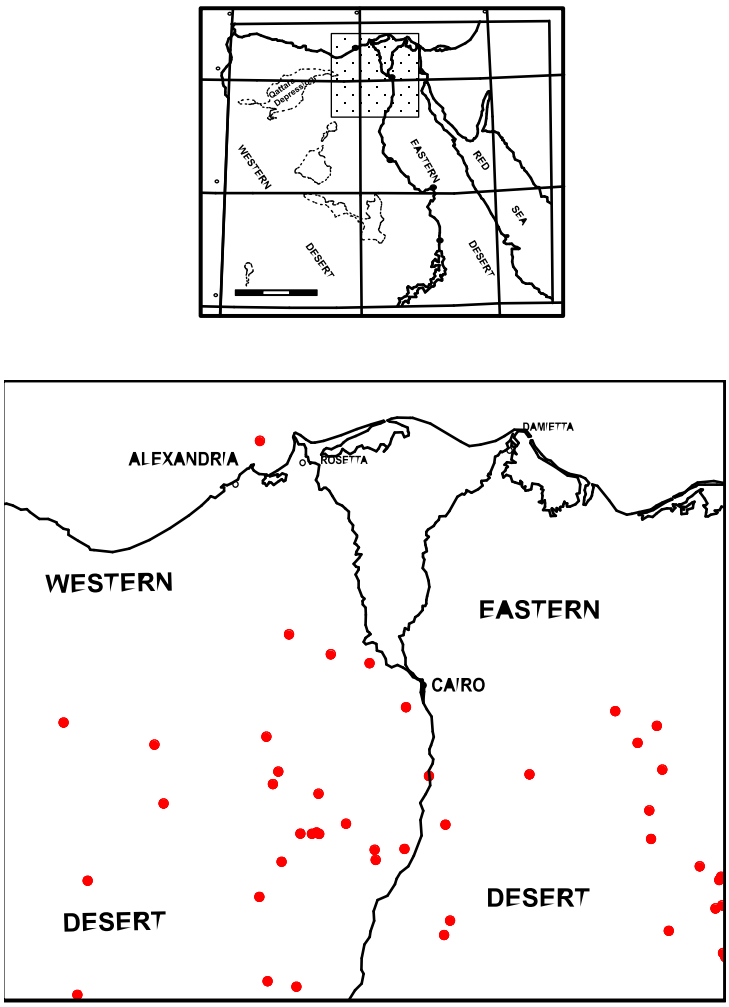

Fig. 1: Location map of the study area, showing the names and locations of the basement bottomed drilled wells.

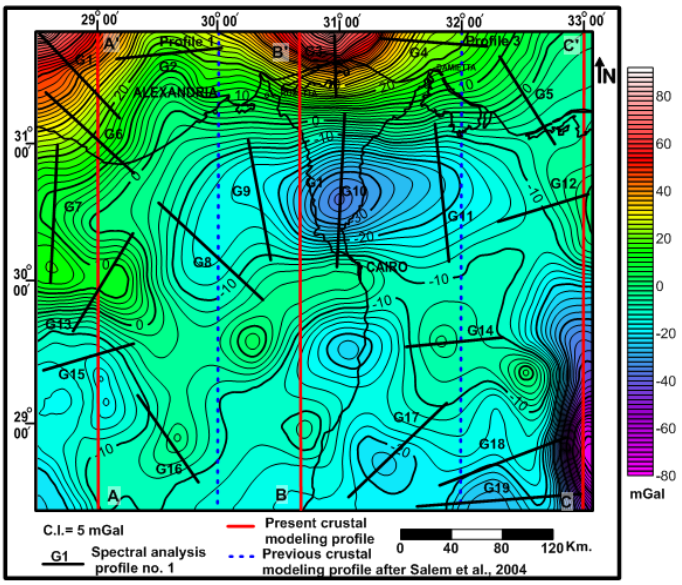

Fig. 2: Bouguer gravity anomaly map, showing the locations of the present and previous crustal modeling profiles [41], as well as the spectral analysis profiles used in depth estimation.

General Geology and Tectonics:

The studied area, being a part of the northern Western Desert, covers the whole Nile Delta and the northern parts of the Eastern and Western Deserts. Its geology belongs to the regional geology of the enclosing region, which was subjected to many cycles of sea regressions and transgressions with varying tectonic activities, which are responsible for giving the area its stratigraphic and structural patterns.

Structurally, it is well known that, the whole northern Egypt lies within the unstable mobile belt of the tectonic framework of the Egyptian Territory [39]. Consequently, it is characterized by deep and rugged basement rocks, thick sedimentary succession of highly printed complex structural effects represented by asymmetric linear folding, faulting and diaprism resulted from considerable and varying tectonic disturbances. Many workers, such as [39,4,5,23,24,25,11,45,13,41] and others, are dealt and still dealing with these structures. They were searching about the surface and subsurface conditions controlling the most important features distributed along this region.

The surface geology of this area consists of Mesozoic to Tertiary sediments in the southern parts, and Miocene - Pleistocene sediments in the northern parts, with sand dunes, mud, silt and sabkha, covering this region up to the Mediterranean coast [41].

Structurally, Northern Egypt has suffered from all stresses effecting the pre-Cambrian up to the Recent, where the sedimentary cover has been signed by most of the resulted deformational tectonics, from Paleozoic up to the Recent. The structural grains, according to many workers [39,25,27] comprise faulting, uplifting, folding, subsidence and other tectonic features, which have been printed out by different stresse effects. Uplifting, normal and transform faulting associated with the Red Sea rifting, as well as uplifting of the Northern Nile Delta associated with the Gulf of Suez events during Middle Miocene age [19] have been investigated. Miocene subsidence and Aqaba fault systems (Late Miocene to Paleocene) are also inferred.

According to the generalized litho-stratigraphic column of Schlumberger [42] for the Nile Delta, which depending mostly on the geologic sections correlation, the thickness of the Pre-Miocene formations ranges approximately from 2 to 3 km, whilst the formations thickness of the Miocene to Recent varies between 3 and 6 km. Hence, the total sedimentary cover occupying the Nile Delta and the Nile Cone speculatively varies from 5 to 9 km, except at Abu Roash area, that situated south of the Nile Delta block, where the Mesozoic sediments are cropping out. The depth to the basement at this part is about 1.9 km [39].

Results and Discussions

Analysis of Bouguer Anomaly Map:

The present study is based mainly on the gravity data, aided by the available drilled wells within the area. The gravity data utilized in this study is represented by Bouguer gravity anomaly map with scale of 1:500,000 and contour interval of one mgal (Fig. 2), measured by the Egyptian General Petroleum Corporation (EGPC) in 1980. The interpretation of such a map is extremely useful for determining the depths and relief of the basement surface, Conrad and Moho discontinuities of the area. This map is subjected to both qualitative and quantitative interpretations.

Qualitative interpretation:

Qualitatively, the Bouguer gravity anomaly map (Fig. 2) of the study area reveals a series of positive and negative gravity anomalies with different sizes, shapes, trends and extensions, with nearly uniform or gentle gradients allover the study area, except for the northern part, in which sharp linear anomalies are more or less parallel to the shoreline of the Mediterranean Sea with maximum amplitude of 80 mGal to the north and in the southeastern corner with minimum amplitude of -75 mGal trending in the N-S direction. These sharp linear anomalies occurred in the northern part with high gradients may be due to the transition zone surrounding the African plate, where shallower Conrad and Moho discontinuities are expected. A large negative gravity anomaly, trending in the E-W direction lies at the southern part of the Nile Delta, north of Cairo. This negative gravity anomaly with amplitude -33 mGal, may be attributed to the huge sedimentary cover. Meanwhile, the high ones may reflect the basement relief irregularities, as well as the shape and composition of the crustal layer, respectively; because of the relative regional nature of the contours, that extend, at least for more than 400 km in the study area. The trends of the anomaly contours are mostly in the E-W, ENE-WSW and N-S directions.

Faults are generally the most predominant structural elements affecting the study area. They are located at the zones of maximum gradients of the Bouguer anomalies, where the contour lines are denser. The directions of the down-thrown sides of the faults are taken as the directions of decreasing values of gravity contours [6].

Analysis of tectonic trends:

The Bouguer anomaly map (Fig. 2) indicates that, the area under study is characterized by a complex pattern of major and minor faults. In order to enhance, quantitatively, the lengths of the detected anomaly trends, using Affleck's [6] technique, as

measured in the unit of the map scale, their directions around the north (clockwise and anticlockwise) are determined in a 10 spectrum, the total lengths and the total numbers for all the trends are summed up. Table (1) shows a comparison of these grades, numbers and lengths for them. Block diagrams (Fig. 3) are also constructed to illustrate the azimuth-length distributions of them. They show clearly that, N-S (Nubian or East-African), NE (Tibesti or Aualitic or Bukle), NW (Suez, Red Sea or Clysmic), NNE (Aqaba), ENE (Syrian Arc, Qattara or North Sinai folds), E-W (Tethyan or Mediterranean) and WNW (Najd or Darag) trends are affecting the study area [1,14,18,27].

Table 1: Parameters of the major fault trends detected from the Bouguer anomaly map.

WEST					Azimuth	EAST				
N	N%	L	L%	L/N		L/N	L%	L	N%	N
5.0	17.9	401.7	17.4	80.3	0:<10	86.5	3.8	86.5	3.6	1.0
2.0	7.1	161.8	7.0	80.9	10:<20	0.0	0.0	0.0	0.0	0.0
2.0	7.1	193.6	8.4	96.8	20:<30	71.2	9.3	213.7	10.7	3.0
2.0	7.1	170.1	7.4	85.1	30:<40	165.6	7.2	165.6	3.6	1.0
1.0	3.6	55.2	2.4	55.2	40:<50	58.1	2.5	58.1	3.6	1.0
1.0	3.6	70.1	3.0	70.1	50:<60	141.0	6.1	141.0	3.6	1.0
2.0	7.1	104.4	4.5	55.2	60:<70	0.0	0.0	0.0	0.0	0.0
3.0	10.7	184.5	8.0	85.1	70:<80	124.2	5.4	124.2	3.6	1.0
1.0	3.6	75.9	3.3	96.8	80:<90	98.5	4.3	98.5	3.6	1.0
19.0	67.9	1417.2	61.5		Sum		38.5	887.6	32.1	9.0
∑n	28.0		∑L	2304.8		∑n%	100.0		∑L%	100.0

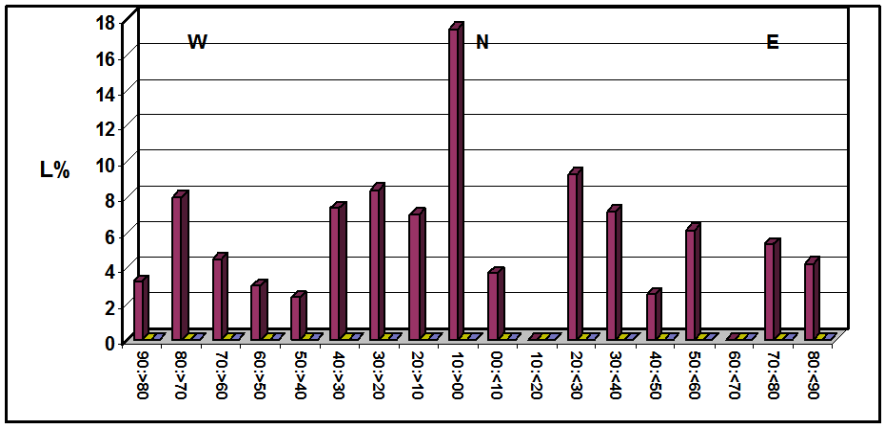

Fig. 3: Block diagram showing the distribution of the fault trends detected from the Bouguer anomaly map.

Isolation of Gravity Anomalies:

To implement the crustal simulation, it is better to remove the effect of shallow-seated causative bodies producing anomalies from the regional ones, in order to show whether the derived long wavelength anomalies map or the original Bouguer one is more reasonable for rational modeling procedures.

Gravity data have been used to study a great many types of geological structure, ranging in depth and size from very deep crustal blocks to near-surface ore bodies. In general, large regional variations in the Bouguer gravity are related to changes in the thickness of the earth's crust or are due to large-scale mass inhomogeneities. Local gravity anomaly values are attributed to the near-surface mass inhomogeneities. Generally, negative anomalies are identified with sedimentary basins, salt and granite structures, and grabens; while positive anomalies are identified with uplifts, horsts and mafic rocks masses.

In the present study, seven orders of the least-squares polynomial technique are used to separate the Bouguer gravity anomaly map into regional and residual components. Higher orders of the least-squares polynomial methods are applied, but they show disagreeable results for both the regional and residual surfaces. Abdelrahman *et al*. [3] and Zeng [52] showed that, the regional surface of this method at the fifth and/or sixth order is related to the upper mantle effect and is similar to the upward continuation at 40 to 45km height.

Figure (4) shows the third-order regional polynomial trend surface map. It indicates that, this order is more compatible with the predominant regional pattern than the first and second orders. Generally, this order gives rise to larger-scale anomalies of deep-seated occurrence, consequently expresses this regional nature. There are linear anomalies trending in the E-W direction in the northern part with increasing magnitudes (of about 74 mGals) to the offshore part, due to the transition zone surrounding the African plate, while the negative anomalies (of about -54 mGals) trending

in the E-W and N-S is to the south inside the continental plate. The residual map of the third-order polynomial of the Bouguer anomaly map (Fig. 5) illustrates a good separation of the residual component, where the positive and negative closed anomalies are well represented, as compared to the original Bouguer one. Correlation coefficients results show that, this map is the optimum one, where it has the maximum value of 0.89836, as shown in table (2). The residual map, as shown in figure (5), shows a large negative anomaly north of Cairo (about 80 km) trending in the E-W direction, with amplitude of -23mGal.

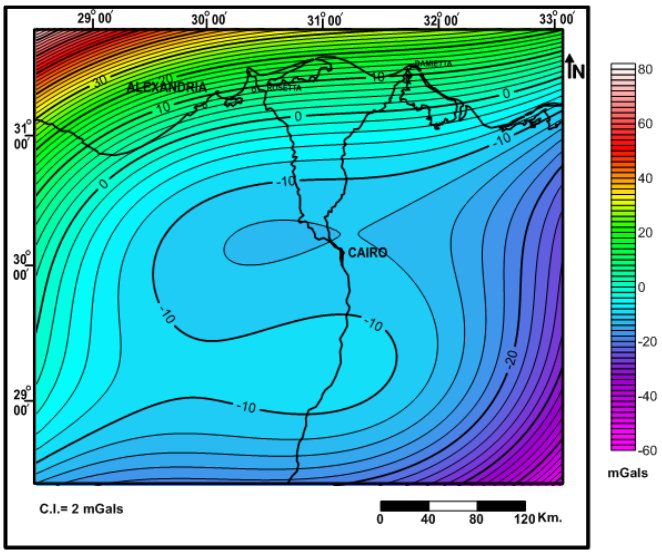

Fig. 4: Regional trend surface of the Bouguer anomaly map with the third order polynomial.

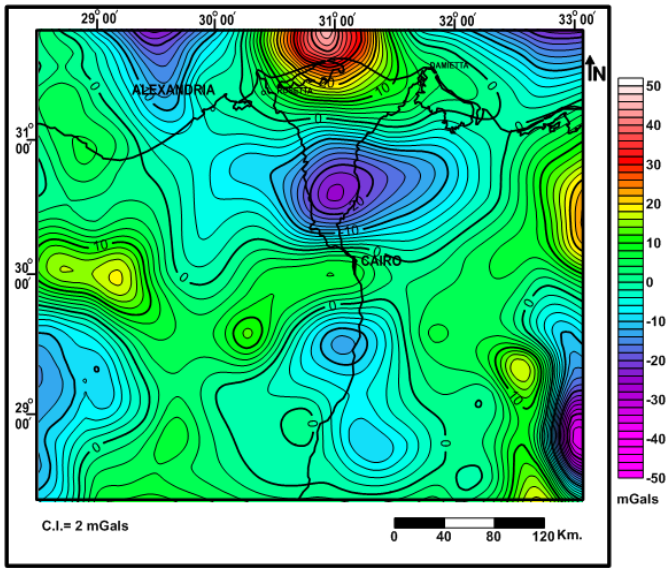

Fig. 5: Residual Bouguer anomaly map with the third order polynomial.

Table 2: Correlation coefficients resulted form the gravity residual maps, using the least-squares polynomial technique.

	1st order	2nd order	3rd order	4th order	5th order	6th order	7th order
1st order	1						
2nd order	0.87696	1					
3rd order	0.71739	0.81789	1				
4th order	0.64254	0.73268	0.89836	1			
5th order	0.37274	0.4272	0.51849	0.54089	1		
6th order	0.35778	0.41668	0.48053	0.53321	0.54917	1	
7th order	0.35342	0.4097	0.48455	0.52807	0.74092	0.82029	1

Another negative anomaly with an ENE trend lies to the south of Cairo (about 80 km) on the Nile Valley. Four negative anomalies are shown in the corners of the study area trending in the N-S direction. The western side is characterized by positive anomalies trending NNW and E-W. The extreme southern strip of the map, with a positive anomaly trending in the E-W. While the eastern part of the map shows a positive trending in the N-S and NW may be due to the highs of El-Galala El-Baharyia. The maximum amplitude of 45 mGal is shown north of the area, between Rosetta and Damietta.

Depth Estimation Methods:

The results of depth estimation can supply information concerning the thickness of the sedimentary succession. Consequently, it is possible to delineate the configuration of the sedimentary basins in the study area and to give an idea about the topography of deeply buried basement. Nineteen profiles covering almost the study area are used to estimate the depths to the basement surface using the spectral analysis technique [44]. The locations of these profiles are shown in figure (2). A figure (6) illustrates two examples for the spectral analysis calculation along profiles G7 and G17. All the results of spectral analysis technique are tabulated in table (3). This table shows that, the basement depths range from 2.5 km at the southwestern corner (profile G16) to about 8.3 km at the main basin in the northern part (profile G10). The Conrad depths range from about 13 km north of Damietta (profile G4) to about 22 km at the western part (profile G13), while the Moho discontinuity depths range from 21.5 km in the northeastern corner (profile G1) to 33.7 km at the southwestern corner (profile G16). Generally, the Conrad and Moho depths are shallow at northern profiles, where these profiles have high magnitudes, as comparable with the gravity map.

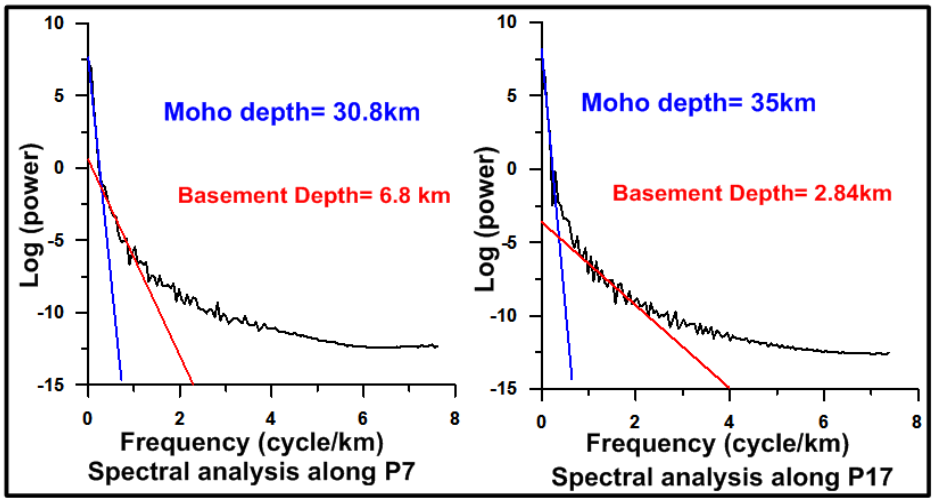

Fig. 6: Spectral analysis along profiles P7 and P17 as examples (using [44]).

Table 3: Results of depth estimation using spectral analysis technique.

Profile name	Basement depth (km)	Conrad Discontinuity depth (km)	Moho Discontinuity depth (km)
G1	7.7	-	21.5
G2	7.5	-	22.6
G3	4.91	-	22.3
G4	6.4	12.87	-
G5	4.51	16.2	-
G6	5.6	14.2	-
G7	6.8	-	30.8
G8	4.2	-	28.7
G9	5.4	-	29.4
G10	8.3	-	30.8
G11	6.7	-	29.5
G12	6	19.3	-
G13	3.8	22.2	-
G14	4.98	-	30.8
G15	4.5	-	30.8
G16	2.5	-	33.7
G17	2.84	-	35
G18	2.99	22.7	-
G19	2.76	21.8	-

Euler Deconvolution:

Figure (7) shows the application of the Euler deconvolution technique on the Bouguer gravity data, to illustrate the distribution of the step-faults and to define their locations and depths at different levels of calculations. This technique is carried out using the Geosoft, software with SI = 0 (gravity step, Barbosa *et al*., [7]) and window size = 10. It shows step-faults running in the N-S, E-W, ENE and NW-SE directions. The step-faults around the basins and/or up-lifted blocks have depths range from zero to 9 km. Correlation between this map and the Bouguer gravity map reveals that, the step-faults are concentrated around the positive and negative anomalies, which qualitatively interpreted as uplifted and down-lifted blocks.

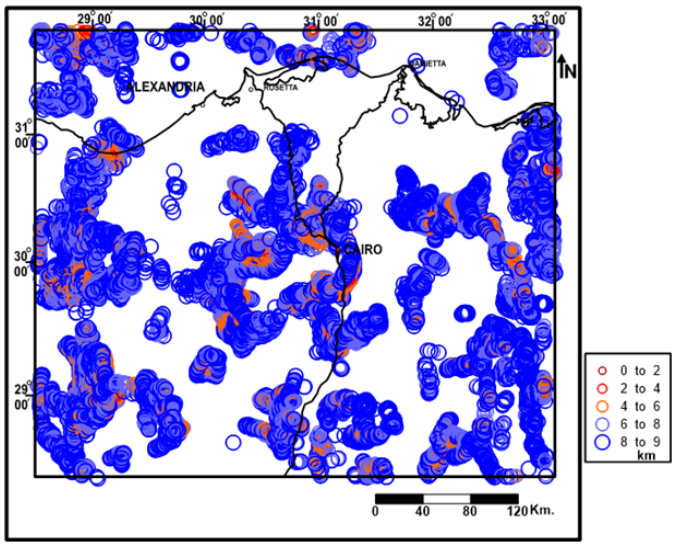

Fig. 7: Step-faults with the locations at depths range from zero to 9 km, using the Euler deconvolution.

Gravity Modeling:

Generally, gravity data indicate that, there is a regular relationship among crustal structure, crustal density (composition) and surface elevation. For regional scale, Bouguer anomalies may be sufficiently clear to give evidence of changes in mass discontinuities in the crust and upper-mantle, as well as the distribution of isostatic balance [48]. Recent studies indicate that, the Bouguer anomalies and surface relief are closely connected with the crustal thickness [50,34,36,37]. However, gravity data alone cannot yield unique solution for density distribution in the earth's interior [49].

2-D Gravity Modeling:

According to Woollard [50], the inspection of this suggested density model depicts that, the density of the upper mantle layer is 3.33 g/cc accords with the known upper mantle density (3.32 g/cc) of the continental plateaus. Concomitantly, the lower crust density is 2.93 g/cc in this model, as close to fall in the known range of 2.86- 2.88g/cc. Moreover, the density contrast between the lower crust and the upper mantle is 0.4 g/cc in agreement with the known range of 0.4-0.45 g/cc for this sharp discontinuity to continuous surface and nearly universe marker reflectance of the upper mantle (Moho). Finally, the upper crust - lower crust density contrast is 0.23 g/cc more appropriate for such relatively faint discontinuity (Conrad) second order surface and/or zone. Hence, these outlines manifest that, the suggested density model seems to be justifiable [41].

So, in the present study we use the same density values to construct the 2-D gravity models. I.e., 2.1, 2.5, 2.7, 2.93 and 3.3 g/cc for the upper sedimentary cover, lower sedimentary cover, upper crust, lower crust and Upper Mantle, respectively.

The gravity profiles (AA′, BB' and CC′, Fig. 2) trend in the S-N direction, in order to study the nature of the crust, using 2-D GM-SYS program, that based on Talwani and Heirtzler [47] algorithm. Three profiles have been selected for the modeling approach, Each profile has been simulated by a new 2-D density. Therefore, three 2-D crustal geologic sections, along the selected gravity profiles, are obtained from the modeling procedures after numerous iterations, these sections are inferred in figures 9, 10 and 11.

Three drilled wells reached to the basement are located close to profile AA' (Fig. 8), namely Baharyia-1, Diyure-1 and Rabat-1 wells at 4, 74 and 170 km, respectively, from starting points at the south, as shown in figure (2) and table (4). The basement depths vary from about 1km in the south to about 9 km in the middle part and reaches 7 km in

the northern portion. While the second profile BB' has one basement well (Qarun 2-1), lies at 109 km from south, with a basement depth of 3.1km, and the other one is very close (Natrun Ghibli E.) and lies at 211 km from the south, with a depth of 4.5 km to the basement surface, as shown in table (4). In figure (9), the modeled basement depths show depths range from 2 to 8 km. Also, the third profile CC' has seven basement wells (Figs. 1 and 2), namely from south to north, Bel M-57, Bel MNW-1, GS 184-1, AZ 11-1, DD 84-1, Abu Zenima-1 and Hb 80-1. Their basement depths range from 3.26 to 4.48km, as shown in table (4). In figure (10), the modeled basement depth shows depths range from 2 to 9 km. Conrad discontinuity has depths range between 13 and 24 km in the three models. They show a noticeable thinning of the upper Crust from south to north. In addition, the Moho discontinuity has the same behavior, where the depths range between 19 and 33 km in these models, revealing visibly crustal stretching and thinning northerly. This can be interpreting the high amplitude observed at these profiles to the northern parts.

Two profiles, namely profiles 1and 3, are constructed, after Salem et al., 2004 (Fig. 11). The locations of these profiles are shown in figure (2).

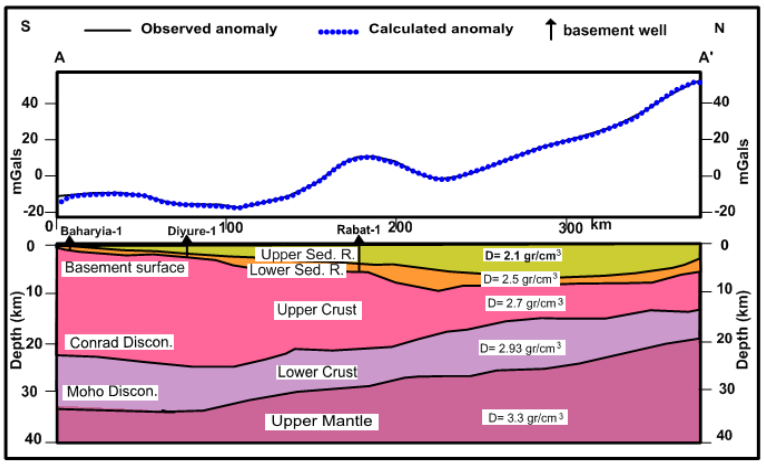

Fig. 8: Crustal modeling along profile AA'.

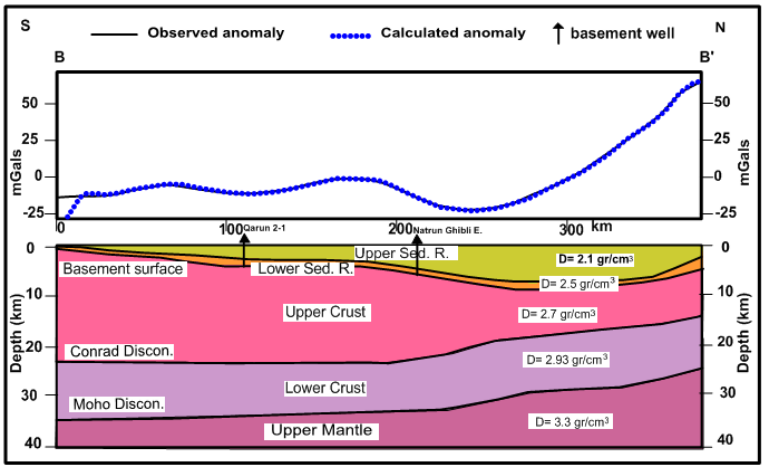

Fig. 9: Crustal modeling along profile BB'.

Construction of the Crustal Maps:

The main purpose of these maps is to focus on the depths change of the basement surface, as well as Conrad and Moho discontinuities. Three maps are constructed, depending on the available wells reached to the basement and the data derived from the depths estimated using the spectral analysis technique, as well as the data resulting from five 2D-gravity models. These maps are the basement depth map, Conrad and Moho Discontinuities depth maps.

1-a- The Basement relief map:

In this map, 46 drilled wells reached to the basement surface as shown in figure (1), which are listed in table (4) and the calculated depths to the basement deduced from 19 gravity profiles, as shown in table (3), are used to construct this map. The

locations of these profiles is illustrated in figure (2). In addition, the depths of the basement surface are digitized and used to construct the basement map. Three profiles (AA', BB' and CC') are carried out in the present work, as shown in figures 8, 9 and 10, while two profiles (1and 3) are constructed after Salem *et al*., [41].

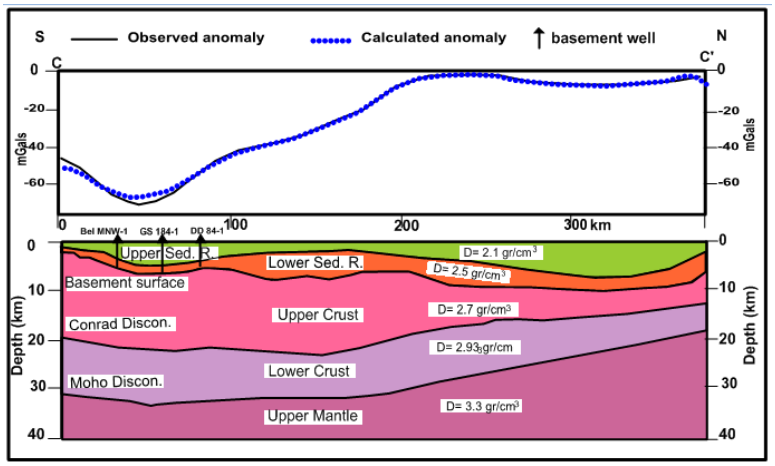

Fig. 10: Crustal modeling along profile CC'.

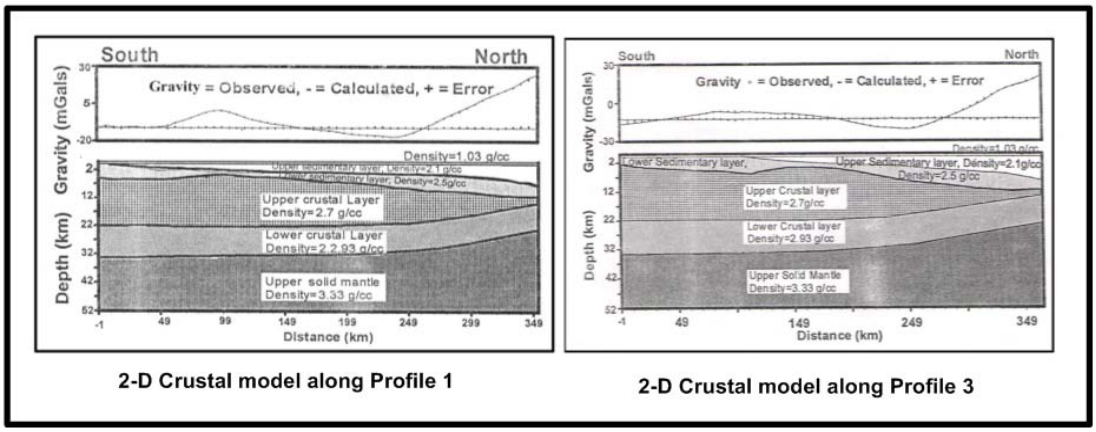

Fig. 11: 2-D Crustal model along Profiles 1 and 3 (After Salem *et al*., [41]).

The basement relief map (Fig. 12) shows a general increase in depths from south to north, i.e. the sedimentary basin thickness increases northward. The minimum value is shown in the southwestern corner of about 1km. The area south of latitude 30^{o} has a basement depth less than 5km. Moreover, the northwestern and northeastern corners, as well as the area north of Cairo have depths more than 7 km.

1-b- The Conrad depth map:

This map is constructed from the five gravity profiles shown in table (3) and the digitized depths of the 2D-gravity modeling along these profiles.

The Conrad depth map (Fig. 13) shows a general decrease toward the north. Generally, the Conrad depths range from about 13.5 at the northern parts to 24km at the southern area. The area south of Latitude 30 has depths larger than 22km the area around Latitude 30^{o} 30' shows sharp depth change, which can be considered the beginning of rapid change to transition of more basic zone, as compared with the Bouguer gravity anomaly map (Fig. 2).

1-c- The Moho depth map:

This map is constructed from the fourteen gravity profiles shown in table (3) and the depths of the 2D-gravity modeling profiles.

The Moho depth map (Fig. 14), to some extent has considerable analogy to the Conrad depth map (Fig. 13), and delineates a general decrease of its depths toward north. The Moho depths range from about 20 to 35km. The maximum depth value lies at the southeastern corner and attains a depth of about 35km, while the minimum Moho depth value locates the northwestern corner and reaches a depth of about 20km.

Table 4: Drilled wells that reached to basement rocks in the study area.

No.	Well name	TD (km)	No.	Well name	TD (km)
1	WADI RAYAN-1X	2.36	24	GHARIBON-1X	2.92
2	NASHFA-1	0.73	25	EL NESR-1X	2.97
3	ATAQA-1	1.20	26	WD 57-1	2.99
4	WADI RAYAN-1	1.29	27	QARUN 2-1	3.10
5	W.BENI SUEF-3	1.30	28	E.W.D 38-1X	3.15
6	DIYUR-1	1.62	29	DD 84-1	3.26
7	EL WASTA-1	1.73	30	ABU ZENIMA-1	3.35
8	BAHARYIA-1	1.84	31	Hb 80-1	3.36
9	KHATATABA	1.91	32	BENI SUEF-1X	3.39
10	ABU ROASH-1	1.92	33	FAYUM-1	3.49
11	BB 80-1	2.03	34	N.B.Q.-2X	3.51
12	WADI RAYAN-2X	2.05	35	RUDEIS-8	3.73
13	W.BENI SUEF-2	2.09	36	FINA Z80-1	3.76
14	W.WADI RAYAN -1X	2.19	37	BEL. MNW-1	3.83
15	RABAT-1	2.20	38	AZ 11-1	3.89
16	LAHUN-1X	2.20	39	KATTANIYA-1	4.06
17	ISSARAN-1	2.22	40	WADI EL NATRUN-1	4.07
18	BRE-6-1	2.27	41	GS 184-1	4.21
19	WADI RAYAN S -1X	2.30	42	E. Bahariya-32A	4.44
20	GS-9	2.53	43	BEL. M-57	4.48
21	WADI GHEIBA-1	2.54	44	NATRUN GHIBLI E.	4.50
22	AYUN MUSA-2	2.59	45	BEL 112 A4	4.86
23	W.SANNUR-1X	2.84	46	S.W WADI RAYAN-1	1.98

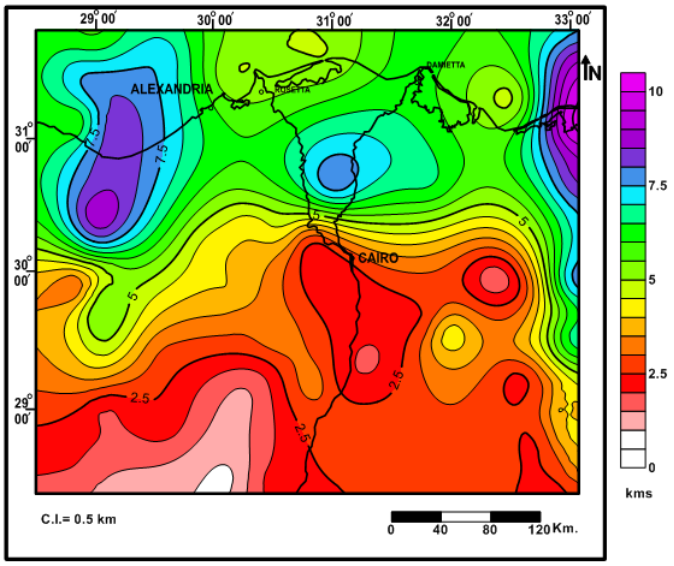

Fig. 12: Basement relief map.

Basement Structures Map:

This map is constructed by integrating all the results obtained from the previous analytical and interpretation techniques on the gravity data of the study area (Fig. 15). It shows two sets of normal faults affecting the study area. These sets are the ENE- WSW to E-W and the NW-SE to NNW-SSE faults represent the major faults, which dominated in the study area. The main fault trend in north Egypt basins is the ENE-WSW trend.

Generally, the area contains many horsts or uplifted blocks belts labeled by H_1, H_2, H_3, H_4 and H_5, as well as grabens or down-lifted blocks belts labeled with L_1, L_2, L_3 and L_4, as shown in figure (15). The ENE to E-W fault system has suffered by later and younger system of transform faulting with Five NW to NNW trends (F_1 to F_5). H_3 can be considering as the main hinge zone, which divided north Egypt into two northern and southern basins. Meshref *et al*. [26] stated that the basement rocks in the northern Egypt has been affected by two fault systems, having large vertical and horizontal displacement, the oldest E-W and ENE trending faults are intersected by youngest NW and NNW trending faults. Therefore, the normal faults are predominant and play the main role in the subsurface basement structures.

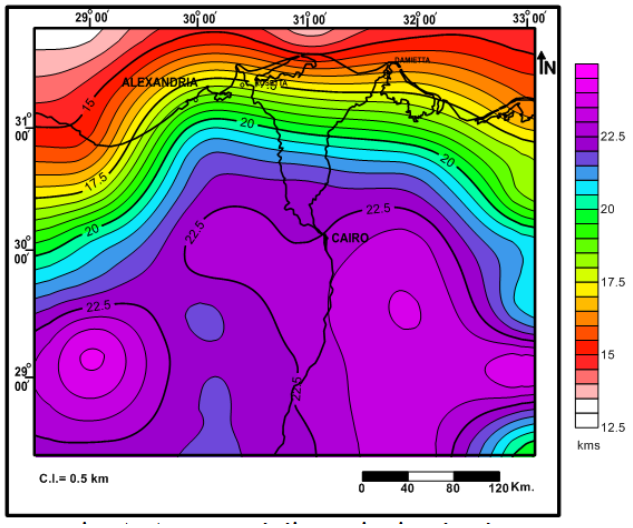

Fig. 13: Conrad discontinuity depth map.

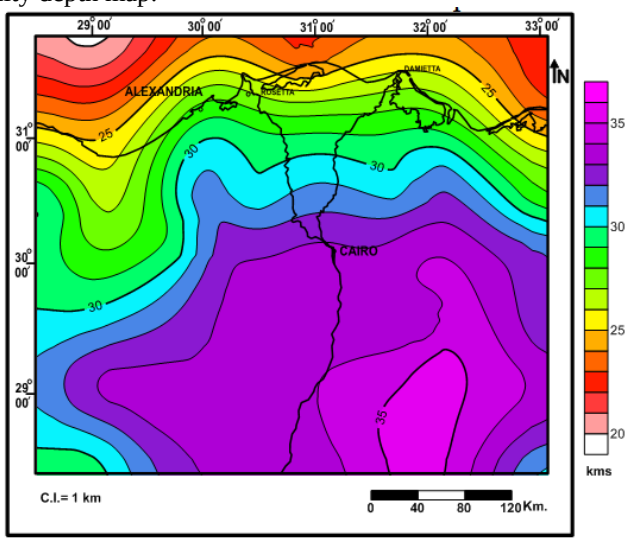

Fig. 14: Moho discontinuity depth map.

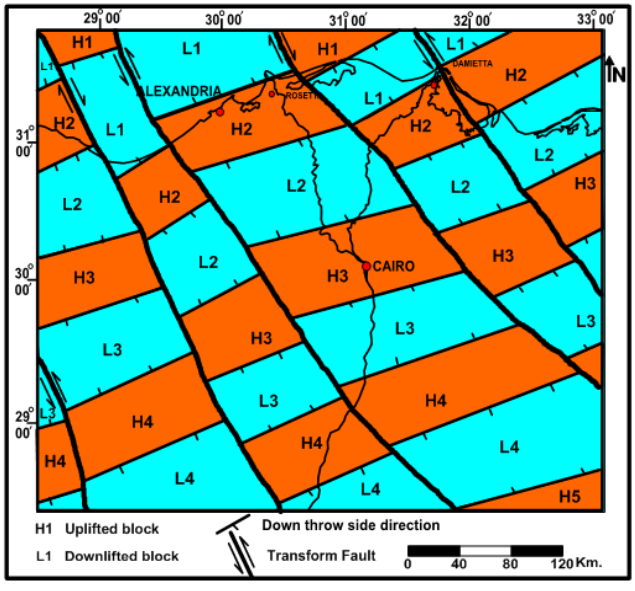

Fig. 15: Interpreted Basement structure map.

Summary and Conclusions:

From the present study, we can conclude that:

1) The trend analysis on the gravity data indicates that, the area is affected mainly by East African (N-S) and Tethyan (E-W) trends with subordinate trends such as ENE, NW, NNE, and WNW trends.

2) The regional – residual separation is applied on the Bouguer gravity map, in order to separate and focus the shallow anomalies (structures) on the expense of the deeper ones. The least-squares polynomial technique of the first to seventh orders is applied. The residual maps of squares polynomial are correlated at the different levels (1^{st} to 7^{th}) by calculating the correlation coefficients. These coefficients indicate that, the regional-residual separation map at the third order is the optimum one of gravity data.

3) The depths to the basement rocks are calculated along nineteen gravity profiles covering almost the study area, using the spectral analysis technique. The depth to basement varies from one place to another. It ranges from 1 to 5 km in the southern part, while in the northern area it attains about 9 km generally the depth increases toward the north.

4) The analysis represents that, the initial simple (two crustal layers overlying the upper mantle) suggested model as 2-D density model of 2.1 g/cc and 2.5g/cc for the upper and lower sedimentary layers. While it shows 2.7g/cc for the upper crustal layer (basement), 2.93g/cc for the lower crustal layer (basaltic layer) and 3.33g/cc for the upper mantle layer, is justifiable.

5) Three crustal models are applied to provide additional information about the deep structures of the crust and upper mantle, as well as to throw more lights on the geometry and evolution of the study area. The basement depth ranges from about 1 to 10 km, while the Conrad Discontinuity varies from about 13.5 to 22 km. The Moho Discontinuity ranges from about 20 to 35 km. It is important to notice that, the thickness of the upper and lower crust decreases from south to north and has the minimum values at the offshore part of the Mediterranean Sea.

6) A basement relief map is constructed using the average depths estimated from the spectral analysis technique (19 profiles), as well as 46 basement wells, in addition to five 2D-gravity models. It shows minimum basement depth in the southwestern corner with a depth of 1km. Generally, this portion has depths range from 1to 2.5 km, while the northern part has depths range from 5to10 km.

7) Conrad and Moho depth maps are constructed, using both the depth estimation profiles and the 2D-gravity models of five profiles. They show noticeable decrease in depths (range from about 13.5 to 24 km and from 20 to 35 km) from south to north.

8) The Euler deconvolution is applied to illustrate the distribution of the step-faults and locate their depths. It shows step-faults running in the N-S and E-W directions, and throughout the area, the step-faults depths range from 0 to 9 km.

9) A basement structural map is constructed, using the integrations of all the results obtained from the previous analytical interpretation on the gravity data. It shows two main fault trends affecting the study area, which are ENE to E-W uplifted and down-lifted blocks belts intersected by the younger NNW to NW, transform faults.

References

1. Abdel Gawad, M., 1970. The Gulf of Suez, a brief review of Stratigraphy and structure. Phil. Trans. Roy. Soc. Lond, A. 267: 23-40.
2. Abdelrahman, E.M., H.M. El-Araby, T.M. El-Araby and E.R. Abo-Ezz, 2001. Three least-squares minimization approaches/to depth, shape and amplitude coefficient determination from gravity data., Geopys., 66(4): l105-1109.
3. Abdelrahman, E.M., S. Riad, E. Refai and Y. Amin, 1985. On the least-squares residual anomaly determinations. Geophys., 50: 473-480.
4. Abu El-Ata, A.S.A., 1981. A study on the tectonics and oil potentialities of some Cretaceous- Jurssic basins, Western Desert, Egypt; using geophysical and suburface geological data. Ph. D. Thesis, Fac. Sci., Ain Shams Univ., 568 p.
5. Abu El-Ata, A.S.A., 1988. The relation between the local tectonics of Egypt and plate tectonics of the surrounding regions, using geophysical and geological data. E.G.S Proc. of 4^{th} Ann. Meet., pp: 103-123.
6. Affleck, L., 1963. Magnetic anomaly trend and spacing patterns. Geophys., 28(3): 379 - 395.
7. Barbosa, V., J. Sliva and W. Medeiros, 1999. Stability analysis and improvement of structural index in Euler deconvolution. Geophys., 64(1): 48-60.
8. Bayoumi, A. and S. Ahmad, 1969. Structural interpretation of geophysical anomalies in Qatrani-El Natrun area. Northern Western Desert, Egypt, the 6th Arab Sc. Congress, Damascuss, Syria, Nov.
9. Bayoumi, A. and S. Ahmad, 1970. A Contribution to magnetic anomalies in the Qatrani-El Natrun area, Northern Western Desert, Egypt, A. R. E., Bull. of Fac. of Sci., no. 44, Cairo University.
10. Cumming, D. and G.L. Shiller, 1971. Isopach map of the earth's crust. Earth Sci. Rev., 7: 97-125.
11. Dennis, S.W., 1984. The tectonic framework of petroleum occurrence in the Western Desert of Egypt, EGPC 7^{th} exploration seminar, Cairo.
12. El-Hadidy, S., A.S.A. Abu El-Ata, R.N. Albert, S. Mustapha and N. Basta, 2000. Shear wave velocity structure of the crust and upper mantle of Northern Egypt; as inferred from multi-mode

surface wave dispersion: part2: constraints of shear-wave-models from surface-wave inversion. Geol. Surv. of Egypt, 23: 389-402.
13. El-Gezeery, R.A., M.A. Saad and S.A. Saada, 2007. Integrated geophysical evaluation of the structural regime of the area southwest of Wadi El Natrun, Weatern Desert, Egypt. Ann. Geol. Surv. Egypt, 29: 299-320.
14. El-Shazly, E.M., M.A. Abdel Hady, A.B. Salman, M.A. Morsy, M.M. El-Rakaiby, I.A. El-Ansary, W.M. Meshref, A.A. Ammar and M.L. Meleik, 1975. Geological and Geophysical investigations of the Suez Canal zone. ASRT, Remote sensing center, Cairo, Egypt.
15. Ghazala, H. EL, I. Korrat, M.R. Sherif and M.M. Belal, 1993. Comparative tectonic study on the Nile Delta using geophysical data. E.G.S Proc. of 11th Ann. Meet., pp: 51-66.
16. Ginzburg, A., J. Makris, K. Fuchs, C. Prodehl, W. Kaminshi and U. Amitai, 1997. A seismic study of the crust and upper mantle of the Jordan- Dead Sea Rift and their transition towards the Mediterranean Sea. Jour. of Geoph. Res., 84(B4): 1569-1582.
17. Gumper, F. and P. Pomeroy, 1970. Seismic wave velocities and earth structure on the African continent. Bull. Seismoi. Soc. Amer., 60: 651-668.
18. Halsey, J.H. and W.C. Gardener, 1975. Tectonic analysis of Egypt using Earth Satellite data. Lecture given to Egyptian Petrol Geol. Cairo. GPC. 23p.
19. Horms, G.C. and J.L. Wary, 1990. Nile Delta in Said (ed.) The geology of Egypt. A.A, Bulkema, Rotterdam, Brokfield, 734p.
20. Keller, G.R. and D.R. Russel, 1980. A crustal structure of the African continent. Ann. of Geol. Surv. of Egypt, 10: 955-960.
21. Makris, J., B. Stoefen, R. Vees, A. Allam, M. Maamun and W. Shehata, 1979. Deep seismic sounding in Egypt, Part (ii). Crust and upper mantle of the Red Sea coast. Unpublished paper, inst. Fur geophysik, univ. Hamburg, 20p.
22. Makris, J., R. Rihm and A. Aharn, 1988. Some geophysical aspects of the evolution and structure of the crust in Egypt. In S. El-Gabi and R. O. Grelling (editors) The Pan African belt of Northeast Africa and the adjacent areas, Viewg, Braunschweig, pp: 345-369.
23. Meneisy, M.Y., 1990. Vulcanicity. in Said(ed.) The Geology of Egypt. A.A., Bulkema, Rotterdam, Brokfield, 734p.
24. Meshref, W.M., 1982. Regional structure setting of the Northern Egypt. EGPC, 6th Exploration Seminar, Cairo, Egypt.
25. Meshref, W.M., 1990. Tectonic Framework of Egypt. A.A., Bulkema, Rotterdam, Brokfield, 734p.
26. Meshref, W.M., S.H. Abdel-Baki, H.M. Abdel-Hady and S.A. Soliman, 1980. Magnetic trend analysis in the northern part of Arabian Nubian Shieldand its tectonic implications. Ann. Geol. Surv. Egypt, 10: 939-953.
27. Moody, G.B., 1961. Petroleum exploration hand book. Mc. Graw. Hill Book Co., 1st Ed., 826p.
28. Morgan, P., 1990. Egypt in the framework of global tectonics in Said.(ed.) The geology of Egypt. A.A., BuSkema, Rotterdam, Brokfield, 734p.
29. Moustafa, A.R. and M.H. Khalil, 1994. Rejuvenation of the eastern Mediterranean passive continental margin in northern and central Sinai: new data from the Themed Fault. Geol. Mag., 131(4): 435-448.
30. Neev, D. and G. Friedman, 1978. Late Holocene tectonic activity among the margins of Sinai subplate, Science, 203: 131-142.
31. Omran, M.A., 1982. Regional Structural Setting of northern Egypt, EGPC., 6th Exploration Seminar, Cairo, Egypt.
32. Omran, M.A., 2000. Crustal modeling of the continental margin of the Nile Delta region. Ann. Geol. Surv. of Egypt, 23: 381-387.
33. Paterson, N.R. and C.V. Reeves, 1985. Application of gravity and magnetic surveys - the state -ofthe- art in 1985. Geophys, 50: 2558-2594.
34. Pick, M., J. Picha and V. Vyskocil, 1973. Theory of Earth`s gravity field. Academia, Publ. Hause of Czechoslovak academy of sciences, Pague, 538p.
35. Reeves, C.V. and I.N. MacSeod, 1983. Modelling of potential field anomalies-some applications for the microcomputer. First Break, 1(8): 18-24.
36. Riad, S., A. Fouad, E. Refai and M. Ghaleb, 1983. Preliminary interpretation of regional gravity anamolies of Egypt. Paper pesented at the eighth General Assembly of the IUGG, Hamburg.
37. Riad, S. and H.A. El-Etr, 1985. Bouguer anomalies and lithosphere- crustal thickness in Uganda. Jour of Geodynamics, 3: 169-186.
38. Robertson, A.H.F., K.C. Eineis, C. Richter and A. Comer Lenghi, 1998. Mesozoic-Tertiary tectonic evolution of Easternmost Mediterranean Sea: Integration of marine and land evidence. Proc. ODP, Sci, Results. 160: College station, TX (Ocean Drilling Program).
39. Said, R., 1962. The Geology of Egypt. Amsterdam, 377p.
40. Said, R., 1981. The Geological Evolution of the River Nile. Springer, Berlin, 155p.
41. Salem, S.R., S.O. El-Khateeb and M.F. Mousa, 2004. Structure and evolution of North African passive margin crust as inferred from 2-D gravity modeling of Nile Delta and its surrounding areas, Egypt, EGS Journal, 2(1): 17-29.

42. Schlumberger, 1984. Egypt Well Evaluation Conference (WEC), Cairo, Egypt, Smith, Ch. M. (editor).
43. Sitto, A.A., 1991. A crustal model for Nile Delta, Egypt. Egypt. J. Geol., 34(1-2): 279-292.
44. Spector, A. and F.S. Grant, 1970. Statiatical models for interpreting aeromagnetic data. Geophys., 35: 293-302.
45. Sultan, N. and M. Abdel Halim, 1988. Tectonic framework of northern Western Desert, Egypt and its effect on hydrocarbon accumulations ; 9th E.G.P.C. exploration conference, CONOCO.
46. Talwani, M. and J.R. Heirtzler, 1964. Computation of magnetic anomalies caused by two-dimensional structures of arbitrary shape. Computer in mineral industries, Standford Univ. Publ., Geol. Sci., 9(1), edited by G.A. Parks.
47. Talwani, M., J.L. Worzel and M. Landisman, 1959. Rapid gravity computation for twodimensional bodies with application to the mendocino submarine fracture zone. J. Geophys. Res., 64: 49-59.
48. Tealeb, A. and S. Riad, 1986. Regional tectonics of Sinai Peninsula interpreted from gravity and deep seismic data. E.G.S. Proc. of 5th Ann. Meeting, March, 29-30: l8-49.
49. Tealeb, A. and S. Riad, 1986. Regional gravity anomalis of western Saudi Arabia and their geological significance. E.G.S. Proc. of 5th Ann. Meeting, March. 29-30: 50- 89.
50. Wollard, G.P., 1959. Crustal structure from gravity and seismic measurements. J. of Geoph. Res., 64(10): 1521-1544.
51. Youssef, M.I., 1968. Structural pattern of Egypt and its interpretation, AAPG Bull, 52(4): 602-614.
52. Zeng, H., 1989. Estimation of the degree of a polynomial fitted to gravity anomalies and its applications. Geophys. Prosp., 37: 959-973.